DOI: 10.1002/ejic.200900835

Thermal Decomposition of Ferric Oxalate Tetrahydrate in Oxidative and Inert Atmospheres: The Role of Ferrous Oxalate as an Intermediate

Pavla Hermankova,[a] Martin Hermanek,*[b] and Radek Zboril[c]

Keywords: Solid-state reactions / Thermolysis / Redox chemistry / Synproportionation / Iron

The thermal decomposition of ferric oxalate tetrahydrate $Fe_2(C_2O_4)_3{\cdot}4H_2O$ was studied in dynamic oxidative and inert atmospheres by using a simultaneous thermogravimetric (TG) and differential scanning calorimetric (DSC) analytical device equipped with an evolved gas analyzer (EGA). Solid-state decomposition products formed during the decomposition were analyzed by ^{57}Fe Mössbauer spectroscopy, in situ and ex situ X-ray powder diffraction, and magnetic measurements. In the dynamic inert atmosphere, we observed the formation of a tiny amount of superparamagnetic iron oxide (most likely Fe_3O_4) together with a majority of ferrous oxalate (FeC_2O_4) and remains of undecomposed $Fe_2(C_2O_4)_3$ after the first decomposition step, which finished at 210 °C. The astonishing presence of the oxidic phase at such low temperatures is a highly probable side effect of the main reduction action of the electrons on the Fe^{III} cations in the ferric oxalate structure, thus resulting in the creation of intermediate FeC_2O_4. The final product of decomposition of the FeC_2O_4 intermediate in a dynamic inert atmosphere is a mixture of wüstite (Fe_xO), α-iron (α-Fe), and magnetite (Fe_3O_4). Their proportion accurately reflects actual disproportionation/synproportionation/redisproportionation processes likely encouraged by the preserved size and morphology of the initial ferric oxalate crystals and that are dependent on temperature. In the oxidative atmosphere, the decomposition proceeds in the three overlapped stages that include dehydration, the astonishing reductive formation of FeC_2O_4 as an intermediate, and final decarboxylation to hematite (α-Fe_2O_3). The principal effect of the experimental conditions on the amount of intermediate formation of FeC_2O_4 in the oxidative atmosphere is also discussed and evaluated from the isothermal experiments carried out at 180 °C.

Introduction

The thermally induced decomposition of a suitable precursor in the solid state represents a very simple way of its transformation towards a desired material. The comprehensive knowledge of the decomposition mechanism, with an especial focus on the intermediates that emerge during the transformation, represents key information necessary for the successive preparation of a desired final product that possesses particular properties. The thermal decomposition of metal salts of oxalic acid has been a subject of numerous investigations, especially as an easy way of preparing various metal oxides.[1–14] In recent years, many studies have been published on the thermal behavior of ferrous oxalate (dihydrate), $FeC_2O_4{\cdot}2H_2O$.[15–32] However, much less attention has been paid to ferric oxalate, $Fe_2(C_2O_4)_3$,[33–41] in spite of an interesting phenomenon, which is the formation of a certain amount of ferrous oxalate during its thermally induced decomposition in an inert atmosphere[35,36,38,39] or during irradiation by γ-rays.[40] The reduction of Fe^{III} to Fe^{II} is ascribed to the electron transfer during oxidation of the oxalate group to yield two electrons that consecutively reduce Fe^{III} cations.[35]

It is generally agreed that under the conditions of a dynamic inert atmosphere, the decomposition of hydrated $Fe_2(C_2O_4)_3$ proceeds in two or three main steps. The majority of authors also observed residues of undecomposed ferric oxalate after the first decomposition step.[35,36,39]

Thus Suzdalev et al.[39] described the dynamic decomposition of ferric oxalate pentahydrate $[Fe_2(C_2O_4)_3{\cdot}5H_2O]$ in the three steps that are reflected by corresponding endotherms in the differential thermal analysis (DTA) curve. The first effect with the minimum at 200 °C is ascribed to the process of dehydratation and partial decomposition of dehydrated ferric oxalate to ferrous oxalate: $3Fe_2(C_2O_4)_3{\cdot}5H_2O \rightarrow Fe_2(C_2O_4)_3 + 4FeC_2O_4 + 15H_2O + 4CO_2$. The second reaction step within the range of 220–320 °C is assigned to the decomposition of the rest of ferric oxalate to Fe_3O_4 and α-Fe: $2Fe_2(C_2O_4)_3 \rightarrow Fe_3O_4 + Fe + 6CO + 6CO_2$. Finally, in the last reaction step (at about 400 °C), the decomposition of ferrous oxalate proceeds: $4FeC_2O_4 \rightarrow Fe_3O_4 + Fe + 4CO + 4CO_2$.

However, quite different results were reported by Galway et al.,[35] who identified two weight losses in the TG curve. The first one, between 120 and 190 °C, is ascribed to the overlap of the two processes: salt dehydration and decom-

[a] Moravian College Olomouc,
Jeremenkova 42, 772 00 Olomouc, Czech Republic
[b] Department of Experimental Physics, Palacky University,
17. listopadu 12, 77146 Olomouc, Czech Republic
Fax: +420-585634958
E-mail: martin.hermanek@upol.cz
[c] Centre for Nanomaterial Research, Palacky University,
Slechtitelu 11, 78371 Olomouc, Czech Republic
Supporting information for this article is available on the WWW under http://dx.doi.org/10.1002/ejic.200900835.

position to ferrous oxalate with a small residue of undecomposed ferric salt, the presence of which is concluded from a lower weight loss relative to that that is theoretically expected. The second step, between 190 and 350 °C, is ascribed to ferrous oxalate decomposition to wüstite (FeO), which consecutively disproportionates to Fe and Fe_3O_4. Such a composition was also observed at 900 °C.[34]

However, the results reported for the decomposition of a mixture of $FeC_2O_4 \cdot 2H_2O$ and $Fe_2(C_2O_4)_3 \cdot 5H_2O$ lead to completely different conclusions.[41] The first step of a two-step process is ascribed to the decomposition of ferrous oxalate to iron(II) carbonate: $FeC_2O_4 \rightarrow FeCO_3 + CO$, whereas the second one covers two consecutive reactions: $FeCO_3 \rightarrow FeO + CO_2$ followed by $Fe_2(C_2O_4)_3 \rightarrow Fe_2O_3 + 3CO_2 + 3CO$. It should be mentioned, however, that despite the results concluded from the weight losses, no specific values are mentioned in this work.

Under oxidative conditions, on the other hand, the decomposition of hydrated $Fe_2(C_2O_4)_3$ is far more straightforward, with hematite (α-Fe_2O_3) being the final decomposition product.[34] Various Fe_2O_3 phases (amorphous, γ, and α) were also identified in the case of worsened oxidative conditions (samples in the form of pellets).[37] Moreover, the decomposition in air does not proceed in differentiable stages (dehydration and consequent decarboxylation), but considerable oxalate breakdown takes place although some water still remains in the sample.[33]

The present work resumes our recent investigations on the mechanism of $FeC_2O_4 \cdot 2H_2O$ decomposition,[28–30,32] which represents an intermediate phase in the thermal decomposition of ferric oxalate under inert conditions. As already mentioned, the literature data are quite inconsistent; various intermediates and products are mentioned, and the mechanism of the $Fe^{III} \leftrightarrow Fe^{II}$ transition and the amount of ferrous oxalate that originates during the decomposition of hydrated $Fe_2(C_2O_4)_3$ are also not comprehensively clear. Moreover, in our previous study focused on oxidative decompositions of various organometallic salts including FeC_2O_4 in air, we observed that $Fe_2(C_2O_4)_3$ decomposition was also accompanied by a local sample temperature increase caused by a violent oxidation; in the case of FeC_2O_4, this was unambiguously connected to the increase in the oxidation state of iron.[32] This fact leads us to the assumption that, similarly to that in the inert atmosphere, Fe^{II} cations might also be present in an intermediate during $Fe_2(C_2O_4)_3$ decomposition in air. To the best of our knowledge, this phenomenon has never been published.

Thus, in this work, we attempt to comprehensively describe the decomposition mechanism of $Fe_2(C_2O_4)_3 \cdot 4H_2O$ under inert and oxidative atmospheres with the primary focus on the intermediate formation of FeC_2O_4 in these processes.

Results and Discussion

Decomposition Under Dynamic Inert Conditions

Simultaneous TG and DSC curves of the $Fe_2(C_2O_4)_3 \cdot 4H_2O$ decomposition in the dynamic argon atmosphere are shown in Figure 1. The first weight loss (35.63%) within a range of 120–210 °C is followed by a very slow weight decrease (1.45%) up to 300 °C. The DSC curve shows two endothermic effects with two close minima at 174 and 185 °C within this temperature range that correspond to two processes occurring almost at the same time: dehydration and salt decomposition. Afterwards, there is a steep mass decrease of 30.14% within the temperatures of 300–390 °C in the TG curve accompanied by an intensive endothermic effect with a minimum at 367 °C in the DSC curve. This step can be assigned to the decomposition process. Above 390 °C, no observable weight change takes place. The part of the DSC curve that corresponds to this temperature interval shows a small endothermic effect with a tiny minimum at 576 °C, which can be ascribed to a phase transition. It should be mentioned that the temperature of 577 °C is presented as the Curie temperature of magnetite[42] and a very close value of 570 °C represents a temperature below which FeO is unstable and disproportionates to Fe_3O_4 and α-Fe.[35,43–46] The total weight loss of 67.22% is only a little bit lower than a theoretical mass loss expected for the formation of FeO (67.91%).

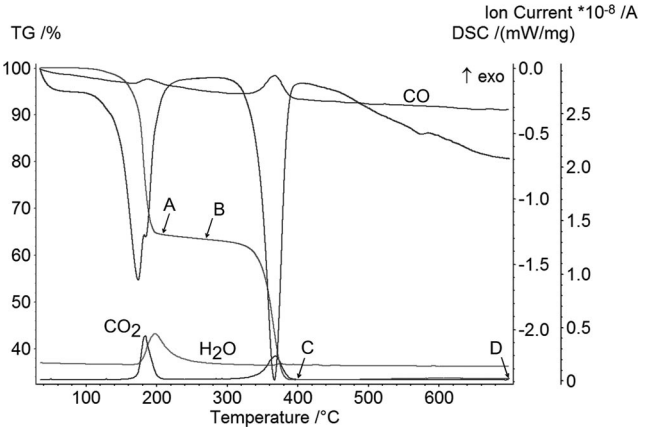

Figure 1. TG, DSC, and EGA curves of thermal decomposition of $Fe_2(C_2O_4)_3 \cdot 4H_2O$ in the dynamic atmosphere of argon.

The above-mentioned conclusions are supported well by evolved gas analysis. The first mass loss in the TG curve is accompanied by three ion-current signals that belong to H_2O (max. 195 °C), CO_2 (max. 184 °C), and CO (max. 185 °C), as clearly demonstrated in Figure 1. Evolution of water confirms well the process of dehydration of hydrated ferric oxalate. The gradually diminishing water-signal intensity indicates that water is present in the sample in a broad temperature interval up to approximately 300 °C. Evolution of carbon dioxide can be unambiguously ascribed to the transformation of ferric oxalate to ferrous oxalate. However, the simultaneous occurrence of CO_2 with CO indicates a breakdown of the ferric oxalate structure that leads to the consequent formation of another, non-oxalate compound. The second weight loss (300–390 °C) is accompanied by a simultaneous evolution of CO_2 and CO, both with a maxi-

mum at 368 °C. This is again in good agreement with the gaseous products suspected to be evolved during ferrous oxalate decomposition in the absence of oxygen with an iron oxide compound as the product.

To find out the phase composition of the sample during the dynamic decomposition, we investigated the chosen representative points (A: 210 °C, B: 260 °C, C: 400 °C, and D: 700 °C) of the TG curve (Figure 1) using Mössbauer spectroscopy, magnetic measurements, and in situ XRD.

The Mössbauer spectrum of sample A (dynamic heating immediately after the first weight loss) is fitted with three doublets (part b of Figure 2, Table 1). The hyperfine parameters of the broadest one (δ = 1.22 mm s^{-1}, ΔE_Q = 2.18 mm s^{-1}), the content of which takes 83.5% of the total spectrum area, are typical for iron(II) and can therefore be ascribed to forming ferrous oxalate.[30] The second, less intense doublet (δ = 0.38 mm s^{-1}) represents clearly the remains of undecomposed ferric oxalate. The third component (shaded) fitted by a tiny doublet (6.3% of spectrum area) possesses the isomer shift value of 0.59 mm s^{-1}, which is evidence of the iron atoms in a mixed Fe^{2+}/Fe^{3+} oxidation state. It could be attributed either to a paramagnetic (non-oxalate/oxidic) or superparamagnetic oxidic compound. However, with respect to its low content in the mixture that results in poorer statistics of the fitted parameters, we cannot determine more precisely the origin of this minor compound in the sample. The fitting procedure of sample A including the detailed hyperfine parameters and statistical data is available in Table S1 in the Supporting Information.

The Mössbauer spectrum of sample B (not shown, Table 1) reflects the phase composition of the sample in the middle of the plateau of the TG curve (dynamic heating up to 260 °C). There is apparently only a tiny change in the quantitative representation of the phases compared with that observed in sample A, especially with respect to further formation of iron(II) oxalate at the expense of iron(III) oxalate. The contribution of the minor phase remains practically unchanged (ca. 6.5% of the spectrum area).

To determine more precisely the origin of the minor compound, created far before 300 °C (the beginning of the second main decomposition step in the TG curve) is reached, we performed magnetic measurements. The zero-field-cooled (ZFC) and field-cooled (FC) magnetization curves of samples A and B are shown in Figure 3. For comparison, ZFC and FC curves of iron(III) oxalate hydrate as well as iron(II) oxalate hydrate are present in the same figure. As clearly seen, both oxalates exhibit curves typical for antiferromagnetic behavior that show a continual decrease of magnetization below ordering temperature. On the other hand, in both samples (A and B), there is evidently an increase in the magnetization at low temperatures (below 17 and 20 K, respectively), which clearly indicates the presence of a non-antiferromagnetic admixture. Apparent deviation between FC and ZFC curves starting at the irreversibility temperature (T_{irr}) is typical for the dynamic behavior of superparamagnetic particles without and in the presence of an external magnetic field.[47] Thus, on the basis of the two above-mentioned facts, the minor component observed in the

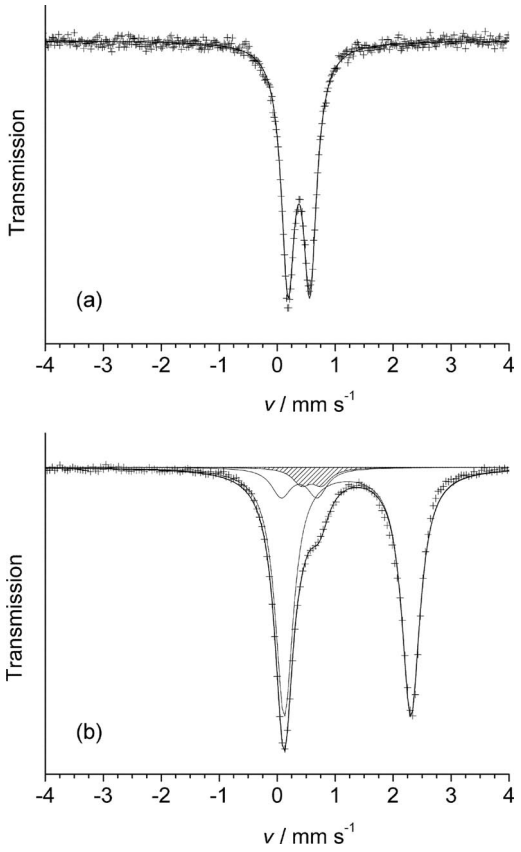

Figure 2. (a) Room temperature Mössbauer spectrum of initial $Fe_2(C_2O_4)_3{\cdot}4H_2O$ and (b) of sample A prepared by dynamic decomposition of $Fe_2(C_2O_4)_3{\cdot}4H_2O$ up to 210 °C in an inert atmosphere of argon and immediately cooled down to room temperature.

Table 1. Room temperature Mössbauer parameters of $Fe_2(C_2O_4)_3{\cdot}4H_2O$ and of samples A and B prepared by dynamic decomposition of $Fe_2(C_2O_4)_3{\cdot}4H_2O$ under an inert atmosphere of argon up to 210 and 260 °C, respectively.[a]

Sample/ T point [°C]	δ[b] [mm s^{-1}]	ΔE_Q[c] [mm s^{-1}]	A_R[d] [%]	Site assignment
$Fe_2(C_2O_4)_3{\cdot}4H_2O$	0.38	0.40	100.0	$Fe_2(C_2O_4)_3{\cdot}4H_2O$
A/210	1.22	2.18	83.5	FeC_2O_4
	0.38F	0.62F	10.2	$Fe_2(C_2O_4)_3$
	0.59	0.35	6.3	mixed Fe^{2+}/Fe^{3+}
B/260	1.21	2.19	87.2	FeC_2O_4
	0.38F	0.65F	6.3	$Fe_2(C_2O_4)_3$
	0.58	0.37	6.5	mixed Fe^{2+}/Fe^{3+}

[a] F: fixed value. [b] Isomer shift (with respect to metallic iron, ±0.01). [c] Quadrupole splitting, ±0.01. [d] Relative spectrum area, ±0.1.

Mössbauer spectra of samples A and B is unambiguously confirmed and can be attributed to a superparamagnetic compound. Moreover, the extremely low value of the blocking temperature (below 5 K) indicates its ultrasmall particle dimension. Taking into account that, from the literature data concerning magnetic behavior of iron-containing compounds, only iron oxides and fluorides are known to behave superparamagnetically, the minor compound could be clearly attributed to a superparamagnetic iron oxide.

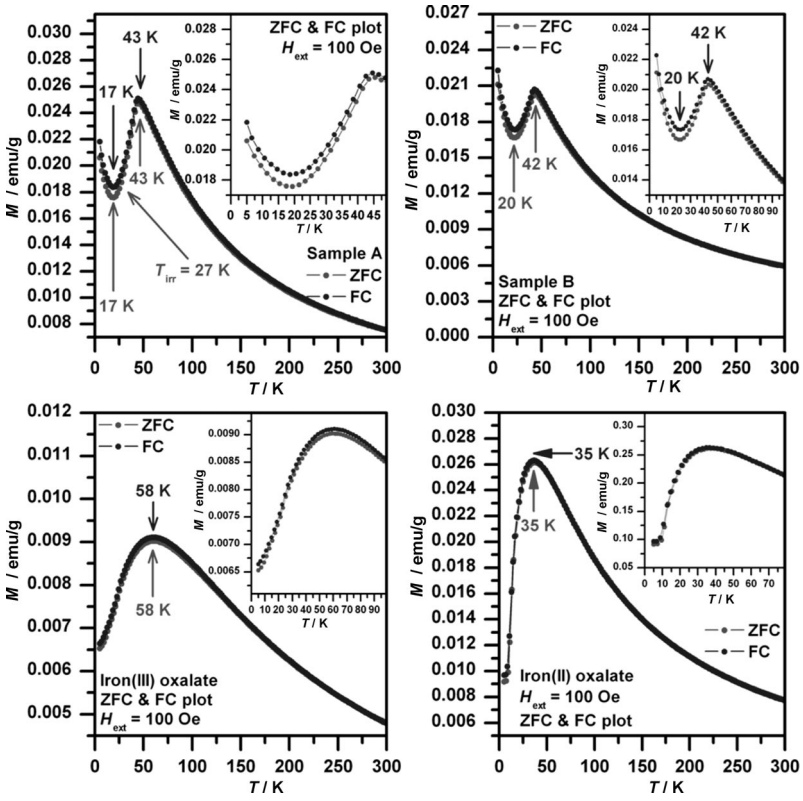

Figure 3. ZFC and FC magnetic curves of sample A, sample B, $Fe_2(C_2O_4)_3{\cdot}4H_2O$, and $FeC_2O_4{\cdot}2H_2O$.

When comparing the magnetization curves of samples A and B, a stronger influence of the superparamagnetic component on the total magnetization is also evident for sample B, as concluded from a decrease of the maximum magnetization value at 43 K (42 K, respectively) and a position shift of the minima of the ZFC and FC curves to a higher temperature (from 17 to 20 K). This could be clearly ascribed to the higher preparation temperature of sample B (260 vs. 210 °C of sample A), which results in better developed particles of the superparamagnetic iron oxide.

Taking into account the phase composition observed at higher temperatures (see below) for a mixture of the oxidic FeO and Fe_3O_4 together with α-Fe, it is highly probable that the origin of superparamagnetic iron oxide will be from the two oxidic compounds. Indeed, in the opposite case there should be an observable transition effect detected in the thermal analysis curves. As FeO in the superparamagnetic state has not been observed so far, the superparamagnetic phase could be most likely attributed to ultrasmall Fe_3O_4. However, the formation of Fe_3O_4 cannot be unambiguously supported by the refined isomer shift of 0.59 mm s^{-1}. At most we can say that this value could correspond to the superparamagnetic species (most likely Fe_3O_4) suggested by the magnetic measurements.

Unexpected formation of the oxidic iron phase at such low temperatures can be explained as follows. Two electrons ($C_2O_2^{2-} \rightarrow 2CO_2 + 2e^-$) are released during each oxalate anion breakdown;[35] for each Fe^{III} cation reduction, however, there is only one electron needed. Hence, a possibility exists that the electrons are in overabundance relative to ambient Fe^{III} cations in some places within the sample volume. In this case, either the reduction of C^{III} cations in the oxalate structure and/or the presence of C^{IV} cations in formed CO_2 might also take place. Both processes could lead to the evolution of CO and therefore cause the formation of the oxidic iron phase observed in this reaction step.

The development of the phases after the second decomposition step (above 390 °C) was investigated by in situ XRD. The in situ XRD pattern of sample C that reflects the phase composition of the sample heated up to 400 °C is shown in Figure 4 (a). There is clear evidence of the narrow diffraction lines of magnetite and α-Fe and the broader lines of wüstite. All these diffractions are shifted to the lower angle values with increasing 2θ, clearly as a consequence of thermal deformation of the unit-cell size.

The in situ XRD pattern of sample D (Figure 4, b) reflects the phase composition of the sample after the completed decomposition process (thermal treatment up to 700 °C). When compared with the previous sample (C), both quantitative and qualitative changes in the phase composition in the temperature interval 400–700 °C are apparent, accompanied by the corresponding endothermic effect at 577 °C in the DSC curve and no change in weight in the TG curve (Figure 1). There are evidently more intensive and far narrower diffraction lines of wüstite and less intensive diffraction lines of α-iron. There is already no evidence of magnetite in sample D.

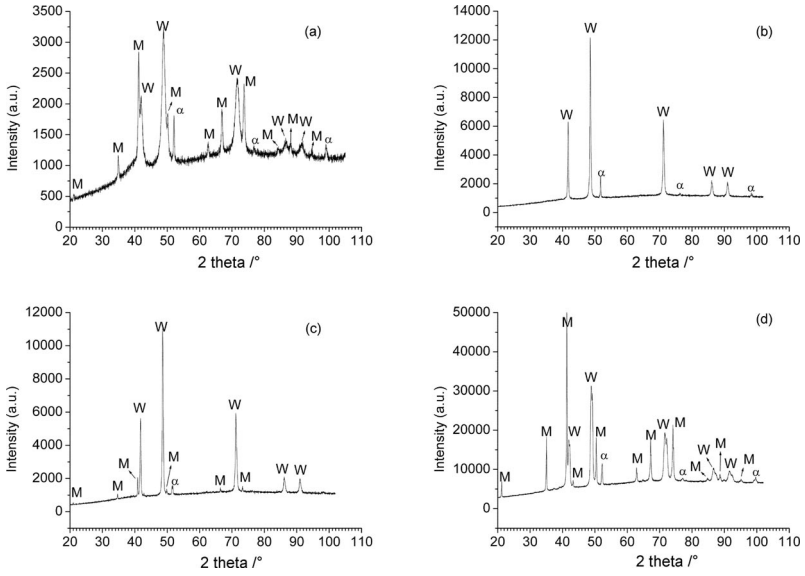

Figure 4. In situ XRD patterns of (a) sample C prepared by dynamic decomposition of $Fe_2(C_2O_4)_3{\cdot}4H_2O$ under an inert atmosphere up to 400 °C, (b) sample D prepared by dynamic decomposition up to 700 °C, and (c) after 120 min at this temperature. (d) Ex situ XRD pattern of sample D dynamically heated up to 700 °C, isothermally treated at this temperature for 120 min, and cooled down to room temperature (25 °C). Diffraction lines assignment: M: magnetite, W: wüstite, α: α-iron.

Thus we assume that wüstite, which immediately disproportionates to magnetite and α-iron, is the principal product of the thermal decomposition of ferric oxalate in a temperature range of 390–570 °C. This is in a good agreement with the theoretical instability of wüstite below this temperature (570 °C).[35,43–46] The idea of formation of FeO as the principal conversion product is also supported by the weight loss of 67.22% observed in the TG curve discussed earlier.

Above 570 °C, on the other hand, a reverse process of synproportionation, namely, $Fe_3O_4 + (4x - 3)\alpha\text{-Fe} \rightarrow 4Fe_xO$, proceeds.[46] At 700 °C, there is already no evidence of magnetite in the in situ XRD pattern, but α-iron is still detected (Figure 4, b). This can be explained by the degree of wüstite stoichiometry; Fe_xO that forms in the range of 300–390 °C is more stoichiometric than that formed above 570 °C. Consequently, that is why not all α-iron is expended to the synproportionation.

The idea that stoichiometric wüstite is formed below 570 °C is concluded on the basis of the fact that only almost stoichiometric wüstite undergoes the disproportionation to Fe_3O_4 and α-Fe,[48] phases we observed in the corresponding XRD pattern (Figure 4, a). The presence of iron-deficient wüstite in the sample above 570 °C is supported by its conversion to iron-richer wüstite and magnetite with time,[44,48] which was observed in the in situ XRD pattern measured after 120 min of the isothermal treatment at 700 °C (Figure 4, c). Hence, an observed decrease in the content of α-iron in this sample can be explained by its partial reaction in forming magnetite.

The XRD pattern of the same sample (D) after cooling to room temperature (Figure 4, d) shows an increase in diffraction line intensities of magnetite and α-iron at the expense of wüstite, which is caused by the redisproportionation process. It proceeds within the interval of thermal instability of wüstite (570–300 °C) and can be attributed, to some extent, to the insufficiently fast cooling rate.[49]

It is worth mentioning that this extreme variation in phase composition observed between in situ and ex situ measurements confirms the considerable complex impact of experimental conditions (temperature, time, heating and cooling rates) in these disproportionation/synproportionation/redisproportionation processes and should be strongly taken into account when interpreting the post-process data. The appearance of the above-mentioned processes can be, to some extent, supported by preserving the size and morphology of initial $Fe_2(C_2O_4)_3{\cdot}4H_2O$ up to the final temperature of 700 °C, as shown in Figure 5. In such a case, all the forming phases (Fe_xO, Fe_3O_4, and α-Fe, all of which possess cubic crystal structures) are probably in a close interaction

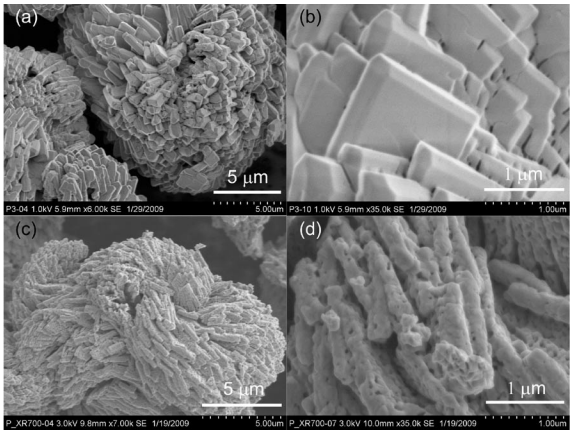

Figure 5. (a), (b) SEM images of $Fe_2(C_2O_4)_3{\cdot}4H_2O$ and (c), (d) of the material dynamically heated up to 700 °C (sample D).

that forms one multiphase composition easily and enables their mutual transformations depending on the momentary equilibrium conditions as discussed earlier. Consequently, it can also be concluded that the proper choice of experimental conditions can lead to the preparation of almost pure phases, and moreover, in the form of crystals that preserve the precursor morphology.

Decomposition Under Dynamic Oxidative Conditions

Simultaneous TG and DSC curves of $Fe_2(C_2O_4)_3{\cdot}4H_2O$ decomposition in the dynamic air atmosphere are shown in Figure 6. It is apparent that the weight decrease is almost straightforward and does not take place in separated distinguishable steps. However, numerous inflection points present on the TG curve indicate more concurrent and overlapping processes. The first weight decrease of 15.35% within the temperature range of 120–180 °C attended by a corresponding endothermic effect in the DSC curve (min. 174 °C) is lower than a decrease assumed for only dehydration (16.09%) and continuously merges into the second steeper loss of weight finishing at 210 °C. This second step is accompanied by a highly intense exothermic effect with a maximum at 200 °C. The final part of the TG curve above 210 °C is characterized by a very slow weight decrease of 0.90%, which is accompanied by a small and relatively broad (400–500 °C) exothermic effect with a maximum at 444 °C in the DSC curve. This caloric effect is not attended by a corresponding change of mass in the TG curve and can be ascribed with high probability to the processes of either crystallization or phase transition. The total weight loss of 64.15% is in good agreement with the theoretical weight loss (64.34%) expected for the formation of Fe_2O_3.

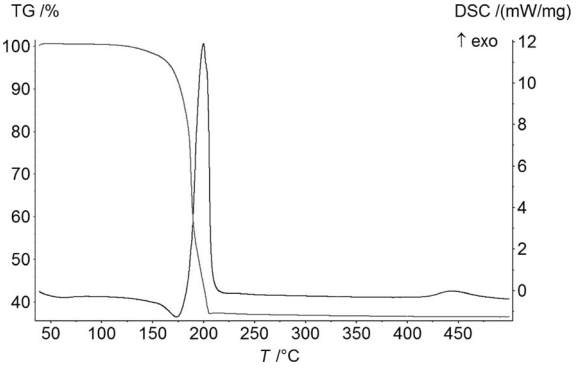

Figure 6. TG and DSC curves of the thermal decomposition of $Fe_2(C_2O_4)_3{\cdot}4H_2O$ in the dynamic air atmosphere.

To find out which processes take place during the steep loss of weight within the short temperature range of 180–210 °C, we stopped the analysis at 185 °C and then rapidly quenched the sample in liquid nitrogen. Afterwards, the material was analyzed by room temperature Mössbauer spectroscopy. Three components, demonstrated by three doublets, were identified in the corresponding spectrum (Figure 7). The narrower doublet with the hyperfine parameters of $\delta = 0.37\ mm\,s^{-1}$ and $\Delta E_Q = 0.66\ mm\,s^{-1}$ can be clearly ascribed to the Fe^{III} cations present in undecomposed ferric oxalate (29.3%). Distortion of its structure, which results as a consequence of thermal effects, is clearly indicated by the increased value of the quadrupole splitting relative to the original value of $\Delta E_Q = 0.40\ mm\,s^{-1}$ that belongs to the precursor (part a of Figure 2, Table 1). Hyperfine parameters of the broadest doublet ($\delta = 1.15\ mm\,s^{-1}$, $\Delta E_Q = 2.25\ mm\,s^{-1}$) match well with Fe^{II} cations in ferrous oxalate. The isomer shift of the third doublet component ($\delta = 0.34\ mm\,s^{-1}$) is typical for high-spin Fe^{III} cations in superparamagnetic Fe_2O_3. A relatively high value of the quadrupole splitting ($\Delta E_Q = 1.17\ mm\,s^{-1}$) provides evidence of highly distorted symmetry of the Fe^{III} nuclei vicinity and indicates therefore the amorphous/poorly crystalline nature of the oxide in the very beginning of the formation.

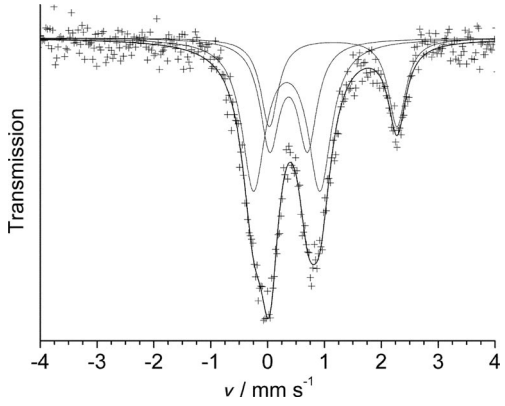

Figure 7. Room temperature Mössbauer spectrum of the sample prepared by dynamic decomposition of $Fe_2(C_2O_4)_3{\cdot}4H_2O$ up to 185 °C in the dynamic air atmosphere.

The observed amount of iron(II) present in the sample heated up to 185 °C is 22.0% of the total spectrum area. It should be emphasized, however, that the decomposition in air proceeds very quickly as follows from the TG and DSC curves (Figure 6). Also the complex phase composition obtained from the Mössbauer spectrum of the sample heated up to 185 °C (Figure 7) indicates several concurrent processes [dehydration of ferric oxalate, intermediate formation of ferrous oxalate, and formation of iron(III) oxide] running almost simultaneously. It might therefore be the reason why the intermediate formation of iron(II) oxalate during iron(III) oxalate decomposition under oxidative conditions has never been observed. Hence, this finding supports the idea that Fe^{III} to Fe^{II} reduction during $Fe_2(C_2O_4)_3$ decomposition is a general phenomenon caused only by the electron transfer and is therefore atmosphere-independent.

Decomposition of $Fe_2(C_2O_4)_3{\cdot}4H_2O$ Under Isothermal Conditions in Air

It is commonly accepted that there are many factors that influence the mechanism and kinetics of solid-state decompositions. Also in our previous study concerning the iso-

thermal decompositions of FeC_2O_4 and other metal salts including Fe^{III} oxalate in air, we demonstrated that a variation of the sample-layer thickness resulted in different conditions of oxygen access into the sample volume.[32] It was reflected through a time-limited increase in the sample temperature in the case of the powder-layer thickness overstepping a certain critical value, which conflicted with the samples decomposing truly isothermally (sample temperature precisely followed the set temperature). In the case of $Fe_2(C_2O_4)_3$, with Fe_2O_3 being the final decomposition product, this observation was quite astonishing, as the exothermal effects accompanied exclusively oxidative solid-state decompositions. Moreover, in comparing the different results with regards to the amounts of observed intermediate FeC_2O_4 formed in dynamic inert and oxidative atmospheres, and taking into account the electronic nature of $Fe^{III} \rightarrow Fe^{II}$ reduction, there is reason to assume that the amount of FeC_2O_4 in an oxidative atmosphere is dependent solely upon the diffusion conditions of oxygen. Thus, we carried out the isothermal experiments for two substantially differing $Fe_2(C_2O_4)_3$ layer thicknesses: sample L (50 mg) and sample H (500 mg), both heated at 180 °C in the same porcelain crucible. The samples were taken out of the furnace at specified time points and quenched in liquid nitrogen. Afterwards, the iron(II) content in as-treated samples was determined using Mössbauer spectroscopy (see Figure 8).

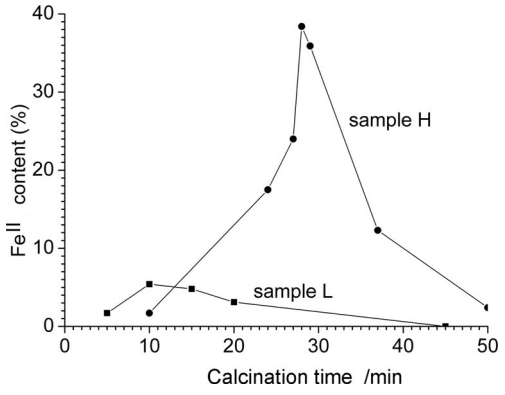

Figure 8. The content of iron(II) oxalate observed during the isothermal decomposition of $Fe_2(C_2O_4)_3 \cdot 4H_2O$ with respect to layer thickness (sample H: 500 mg, sample L: 50 mg).

Thus, it is clear that the less access oxygen has to the sample (the thicker sample layer) the more iron(II) is observed. This result agrees well with our findings for samples under inert conditions, which represent a limit of zero access of air, which results in almost 100% observable reduction of $Fe_2(C_2O_4)_3$ to FeC_2O_4. In other words, the reduction of Fe^{III} to Fe^{II} during $Fe_2(C_2O_4)_3$ decomposition is really a general atmosphere-independent phenomenon, and the amount of FeC_2O_4 observed is strongly dependent upon the rate of its subsequent decomposition to Fe_2O_3.

Conclusion

Intermediate formation of FeC_2O_4 during the decomposition of $Fe_2(C_2O_4)_3$ was clearly proven not only in an inert atmosphere, but also in an oxidative one. Moreover, the amount of detectable FeC_2O_4 under oxidative conditions clearly depends on the access of oxygen to the sample volume. All the intermediates and final products of the decomposition in both dynamic atmospheres were comprehensively described. The significant difference in the phase composition observed between in situ and ex situ measurements was clarified, which positively explains the literature discrepancies. The results can be briefly summarized in the following points:

(1) Under a dynamic inert atmosphere, the decomposition of ferric oxalate to ferrous oxalate following reaction (1) takes place up to 210 °C. A certain amount of ultrasmall iron oxide (most likely superparamagnetic Fe_3O_4) is also formed up to 210 °C; see reactions (1) and (2).

$$Fe_2(C_2O_4)_3 \rightarrow 2FeC_2O_4 + 2CO_2 \quad (1)$$

$$3Fe_2(C_2O_4)_3 \rightarrow 2Fe_3O_4 + 10CO_2 + 8CO \quad (2)$$

Simultaneously, the process of dehydration proceeds up to 300 °C.

Within the temperature range of 300–390 °C, the decomposition of ferrous oxalate formed in the previous reaction step (1a) to wüstite (Fe_xO) takes place; see reaction (3).

$$FeC_2O_4 \rightarrow Fe_xO + CO + CO_2 \quad (3)$$

Thermally unstable Fe_xO undergoes the disproportionation to α-Fe and Fe_3O_4 below 570 °C; see reaction (4).

$$4Fe_xO \rightarrow Fe_3O_4 + \alpha\text{-Fe} \quad (4).$$

Above this temperature, the reverse process of synproportionation proceeds as shown in reaction (5).

$$Fe_3O_4 + \alpha\text{-Fe} \rightarrow 4Fe_xO \quad (5)$$

(2) Fe_2O_3 is the final product of the dynamic decomposition of $Fe_2(C_2O_4)_3 \cdot 4H_2O$ under dynamic oxidative conditions. During this process, FeC_2O_4 is formed as an intermediate product, but its precise quantification is practically impossible due to the fast rate of its decomposition to Fe_2O_3. Isothermal experiments performed under static air conditions proved that the less access oxygen had to the sample volume, the higher the amount of intermediate ferrous oxalate detected.

Experimental Section

General: Dynamic calcinations of $Fe_2(C_2O_4)_3 \cdot 4H_2O$ powder (Sigma Aldrich) were carried out with a simultaneous thermogravimetric (TG) and calorimetric (DSC) analysis device (STA 449 C, Netzsch). The samples were dynamically heated up to chosen temperatures (max. 700 °C) in the dynamic atmospheres of argon and air (both with a flow rate of 30 mL min^{-1}) with a heating rate of 10 °C min^{-1}. Evolved gasses were analyzed (EGA) with a mass spectrometry device (QMS 403 C, Aëolos).

A muffle furnace LM 112.07 (Linn High Therm GmbH) was used for isothermal syntheses at 180 °C. The sample temperature was scanned by a thermocouple, which was in direct contact with the powder.

Solid decomposition products were identified by Mössbauer spectroscopy and X-ray powder diffraction (XRD). Transmission ^{57}Fe Mössbauer spectra of 512 channels were collected with a Mössbauer spectrometer at a constant acceleration mode with a ^{57}Co(Rh) source. The measurements were carried out at room temperature. The isomer shift values were referred to α-Fe. The Mössbauer spectra were fitted with Moss Winn 3.0i xp.

An X′Pert PRO instrument with Co-K_α radiation was employed for XRD analyses within the angle range of 2θ = 0–120°. Phase composition of the samples was evaluated with the X'Pert HighScorePlus software package (®PANanalytical) and JCPDS PDF-4 database. In situ measurements in a nitrogen atmosphere were performed with an Anton Paar reaction chamber XRK900.

SEM images were obtained with a SU 6600 (Hitachi) scanning electron microscope.

A superconducting quantum interference device (SQUID, MPMS XL-7, Quantum Design) was used for the magnetic measurements. The zero-field-cooled (ZFC) and field-cooled (FC) magnetization curves were recorded upon warming samples in the temperature range from 5 to 300 K and in an external magnetic field of 100 Oe after cooling in a zero magnetic field and in a field of 100 Oe, respectively.

Supporting Information (see also the footnote on the first page of this article): Table S1 shows the gradual fitting procedure including statistical data of the room temperature Mössbauer spectrum of sample A prepared by dynamic decomposition of $FeC_2O_4{\cdot}4H_2O$ under an inert atmosphere of argon up to 210 °C. The final fit no. 4 is then presented in Table 1 in the text.

Acknowledgments

This work has been supported by the Projects of the Ministry of Education of the Czech Republic (1M6198959201 and MSM6198959218) and the Academy of Sciences of the Czech Republic (KAN101630651). We warmly thank Jiri Tucek from the Centre for Nanomaterial Research, Palacky University, Olomouc, Czech Republic, for the interpretation of the magnetic measurements and to Walter Horak, Sun Microsystems, Inc., USA, for language correction.

[1] N. Audebrand, S. Raite, D. Louer, *Solid State Sci.* **2003**, *5*, 783–794.
[2] C. J. Cong, L. Liao, J. C. Li, L. X. Fan, K. L. Zhang, *Nanotechnology* **2005**, *16*, 981–984.
[3] K. F. Zhang, X. Z. Sun, G. W. Lou, X. Liu, H. L. Li, Z. X. Su, *Mater. Lett.* **2005**, *59*, 2729–2731.
[4] G. V. Bazuev, O. I. Gyrdasova, *Phys. Status Solidi B* **2008**, *245*, 1184–1190.
[5] N. Deb, *J. Anal. Appl. Pyrol.* **2008**, *82*, 223–228.
[6] E. Drozdz-Ciesla, A. Malecki, B. Jajko, *J. Therm. Anal. Calorim.* **2008**, *92*, 939–944.
[7] L. Duvieubourg-Garea, N. Vigier, F. Abraham, S. Grandjean, *J. Solid State Chem.* **2008**, *181*, 1899–1908.
[8] A. Kumar, J. Kumar, *J. Phys. Chem. Solids* **2008**, *69*, 2764–2772.
[9] X. P. Li, J. D. Wu, M. Wen, X. Tang, Y. Q. Liu, A. L. Xiongping, W. U. Jieda, W. Ming, T. Xiao, L. Yongqiang, *Rare Met.* **2008**, *27*, 598–602.
[10] I. Luisetto, F. Pepe, E. Bemporad, *J. Nanopart. Res.* **2008**, *10*, 59–67.
[11] W. W. Zhou, K. B. Tang, S. A. Zeng, Y. X. Qi, *Nanotechnology* **2008**, *19*, 065602.
[12] F. Davar, F. Mohandes, M. Salavati-Niasari, *Inorg. Chim. Acta* **2009**, *362*, 3663–3668.
[13] P. J. Panteix, V. Baco-Carles, P. Tailhades, M. Rieu, P. Lenormand, F. Ansart, M. L. Fontaine, *Solid State Sci.* **2009**, *11*, 444–450.
[14] M. Salavati-Niasari, N. Mir, F. Davar, *J. Alloys Compd.* **2009**, *476*, 908–912.
[15] V. Rao, A. L. Shashimohan, A. B. Biswas, *J. Mater. Sci.* **1974**, *9*, 430–433.
[16] K. S. Rane, A. K. Nikumbh, A. J. Mukhedkar, *J. Mater. Sci.* **1981**, *16*, 2387–2397.
[17] M. R. Anantharaman, S. S. Shewale, V. S. Rao, K. Seshan, H. V. Keer, *Indian J. Chem. Sect. A* **1982**, *21*, 990–992.
[18] A. S. Brar, K. S. Khabre, *Indian J. Chem. Sect. A* **1982**, *21*, 920–921.
[19] B. Boyanov, D. Khadzhiev, V. Vasilev, *Thermochim. Acta* **1985**, *93*, 89–92.
[20] V. Borker, K. S. Rane, V. Dalal, *J. Mater. Sci. Mater. Electron.* **1993**, *4*, 241–248.
[21] M. A. Mohamed, A. K. Galwey, *Thermochim. Acta* **1993**, *213*, 269–278.
[22] F. S. Li, Y. Kong, D. S. Xue, *Phys. Status Solidi A* **1995**, *148*, 129–133.
[23] Y. Kong, D. S. Xue, F. S. Li, *Phys. Status Solidi A* **1996**, *154*, 553–558.
[24] D. S. Xue, F. S. Li, Y. Kong, J. B. Yang, *J. Phys. Chem. Solids* **1996**, *57*, 461–465.
[25] V. Carles, P. Alphonse, P. Tailhades, A. Rousset, *Thermochim. Acta* **1999**, *334*, 107–113.
[26] M. Popa, J. M. Calderon-Moreno, D. Crisan, M. Zaharescu, *J. Therm. Anal. Calorim.* **2000**, *62*, 633–645.
[27] N. N. Mallikarjuna, B. Govindaraj, A. Lagashetty, A. Venkataraman, *J. Therm. Anal. Calorim.* **2003**, *71*, 915–925.
[28] R. Zboril, L. Machala, M. Mashlan, M. Hermanek, M. Miglierini, A. Fojtik, *Phys. Status Solidi C* **2004**, *1*, 3583–3588.
[29] R. Zboril, L. Machala, M. Mashlan, M. Hermanek, *AIP Conf. Proc.* **2005**, *765*, 257–262.
[30] M. Hermanek, R. Zboril, M. Mashlan, L. Machala, O. Schneeweiss, *J. Mater. Chem.* **2006**, *16*, 1273–1280.
[31] A. Angermann, J. Topfer, *J. Mater. Sci.* **2008**, *43*, 5123–5130.
[32] M. Hermanek, R. Zboril, *Chem. Mater.* **2008**, *20*, 5284–5295.
[33] D. Dollimore, D. Nicholson, *J. Chem. Soc. A* **1966**, 281.
[34] D. Broadbent, D. Dollimore, J. Dollimore, *J. Chem. Soc. A* **1967**, 451.
[35] A. K. Galwey, M. A. Mohamed, *Thermochim. Acta* **1993**, *213*, 279–291.
[36] M. A. Mohamed, M. A. Salem, *J. Anal. Appl. Pyrol.* **1993**, *27*, 275–280.
[37] S. Music, M. Gotic, S. Popovic, I. Czakonagy, *Mater. Lett.* **1994**, *20*, 143–148.
[38] J. Praharaj, S. C. Moharana, S. Bhatta, D. Bhatta, *Indian J. Chem. Sect. A* **2002**, *41*, 1837–1840.
[39] I. P. Suzdalev, A. V. Shkarin, G. M. Zhabrova, V. I. Goldanskii, L. A. Korytko, B. M. Kadenatsi, *Kinet. Katal.* **1966**, *7*, 919.
[40] N. Saito, H. Sano, T. Tominaga, F. Ambe, *Bull. Chem. Soc. Jpn.* **1965**, *38*, 681.
[41] M. E. Mendoza, F. Donado, R. Silva, M. A. Perez, J. L. Carrillo, *J. Phys. Chem. Solids* **2005**, *66*, 927–931.
[42] E. Murad, J. Cashion, *Mössbauer Spectroscopy of Environmental Materials and their Industrial Utilization*, Kluwer Academic, Dordrecht, **2004**.
[43] N. N. Greenwood, A. T. Howe, *J. Chem. Soc., Dalton Trans.* **1972**, 110–116.
[44] S. Stolen, R. Glockner, F. Gronvold, *Thermochim. Acta* **1995**, *256*, 91–106.

[45] A. Pattek-Janczyk, J. C. Grenier, B. Miczko, *Solid State Ionics* **1999**, *117*, 95–103.
[46] F. X. Redl, C. T. Black, G. C. Papaefthymiou, R. L. Sandstrom, M. Yin, H. Zeng, C. B. Murray, S. P. O'Brien, *J. Am. Chem. Soc.* **2004**, *126*, 14583–14599.
[47] J. L. Dormann, D. Fiorani, E. Tronc, in: *Advances in Chemical Physics* (Eds.: I. Prigogine, S. A. Rice), Wiley, New York, **1997**, vol. 98, p. 283.
[48] A. Pattek-Janczyk, *Appl. Catal. A* **1995**, *124*, 267–280.
[49] W. K. Jozwiak, E. Kaczmarek, T. P. Maniecki, W. Ignaczak, W. Maniukiewicz, *Appl. Catal. A* **2007**, *326*, 17–27.

Received: August 24, 2009
Published Online: January 21, 2010

